PAPER

Tunable surface configuration of skyrmion lattices in cubic helimagnets

IOP Publishing Journal of Physics: Condensed Matter
J. Phys.: Condens. Matter **30** (2018) 245001 (12pp) https://doi.org/10.1088/1361-648X/aac288

Tunable surface configuration of skyrmion lattices in cubic helimagnets

Xuejin Wan, Yangfan Hu and Biao Wang

Sino-French Institute of Nuclear Engineering and Technology, Sun Yat-sen University, 510275 Guangzhou, People's Republic of China

E-mail: huyf3@mail.sysu.edu.cn (Yangfan Hu) and wangbiao@mail.sysu.edu.cn (Biao Wang)

Received 15 March 2018, revised 29 April 2018
Accepted for publication 4 May 2018
Published 22 May 2018

Abstract

In bulk helimagnets, the presence of magnetic skyrmion lattices is always accompanied by a periodic stress field due to the intrinsic magnetoelastic coupling. The release of this nontrivial stress field at the surface causes a periodic displacement field, which characterizes a novel particle-like property of skyrmion: its surface configuration. Here, we derive the analytical solution of this displacement field for semi-infinite cubic helimagnet with the skyrmion magnetization approximated by the triple-Q representation. For MnSi, we show that the skyrmion lattices have a bumpy surface configuration characterized by periodically arranged peaks with a characteristic height of about 10^{-13} m. The pattern of the peaks can be controlled by varying the strength of the applied magnetic field. Moreover, we prove that the surface configuration varies together with the motion and deformation of the skyrmion lattices. As a result, the surface configuration can be tuned by application of electric current, mechanical loads, as well as any other effective external fields for skyrmion lattices.

Keywords: skyrmion lattices, surface configuration, magnetoelastic coupling

(Some figures may appear in colour only in the online journal)

1. Introduction

A magnetic skyrmion is a topologically nontrivial spin texture. Periodic arrangement of skyrmions known as skyrmion lattices can be approximated by a superposition of three single-Q helices whose wavevectors form an equilateral triangle, and is thus referred to as a triple-Q structure [1–3]. The existence of skyrmions in helimagnets has been theoretically predicted several decades ago [4, 5], while the first successful experimental observation was achieved in cubic helimagnet MnSi in 2009 [1]. Later, other helimagnets which can host skyrmions were found, such as FeGe [6], $Fe_xCo_{1-x}Si$ [7] and $Mn_{1-x}Fe_xSi$ [8]. In noncentrosymmetric helimagnets, due to the spin–orbit coupling and the lack of inverse symmetry, Dzyaloshinskii–Moriya (DM) interaction arises [9]. Under an appropriate applied magnetic field, the competition between DM energy, favoring spin rotations, and ferromagnetic exchange energy, favoring spin alignment, induces the intriguing skyrmion phase [10]. As a magnetic phase, skyrmions have great potential in the next-generation magnetic storage devices because of their small size, facile current-driven motion [11], and particle-like nature [12, 13].

Magnetic skyrmions share many properties with single particles. They are localized in space and have a long lifetime. They are topologically protected [14, 15], in the sense that the topological integer characterizing them is 1, different from other magnetic structures with topological integer 0, such as helical phase and ferromagnetic phase. They give rise to elementary excitations with rotational mode and breathing mode [16]. Moreover, the system hosting skyrmions may undergo a phase transition from skyrmion phase to skyrmion glass structure [17]. Here we would like to discuss another particle-like property of magnetic skyrmions: their surface configuration.

In helimagnets, interaction between the elastic field and the skyrmion phase due to magnetoelastic coupling occurs in two different energy scales. The strong one is phase-transition-related, for instance, the creation and annihilation of skyrmions in MnSi by uniaxial stress [18, 19] and the jump of elastic stiffnesses C_{11} and C_{33} of MnSi [20]. The weak one is related to the elastic property of the skyrmion phase , for example, the emergent deformation of skyrmion lattices in FeGe induced by anisotropic strain [21] and the periodic elastic field accompanying magnetic skyrmions [22]. For semi-infinite helimagnets with magnetoelastic coupling, the incompatibility between the skyrmion-induced

periodic stress field and the free surface boundary condition will inevitably lead to a displacement field, suggesting that the surface configuration of the material is altered due to the presence of skyrmions.

In this paper, we derive the analytical solution of displacement field for semi-infinite cubic helimagnets hosting skyrmions. Due to magnetoelastic coupling, the peculiar magnetic structure of skyrmions will induce incompatible eigenstrains and further lead to eigenstresses. At the surface, to meet the stress-free requirement, a fictitious force distribution F is applied to balance the eigenstresses, which causes a surface-induced displacement field. Therefore, the total displacement field for semi-infinite cubic helimagnets hosting skyrmions is composed of a skyrmion-induced displacement field and a surface-induced displacement field. The former part has been derived in one of our previous work [22], while the latter part is to be solved here. The elasticity problem induced by F can be decomposed into several plane strain problems and several 3D problems.The 2D plane strain problems are solved by using the Airy stress function and Fourier transform.The 3D problems are solved by taking a harmonic form of the solution. The analytical displacement field is finally obtained by combining the two parts of solution together. For MnSi, the normal displacement field is found to be dominated by two triple-Q structures u_3^{s1} and u_3^{s3}. u_3^{s1} undergoes a 'configurational reversal' and u_3^{s3} remains almost unchanged when the external magnetic field increases from 0.1 T to 0.275 T, resulting in varying surface configuration characterized by periodically arranged peaks. We further demonstrate that the surface displacement field moves or deforms with the motion or deformation of skyrmion lattices. Hence, this displacement field characterizes the surface configuration of skyrmion lattices in general conditions, and is tunable by various kinds of applied field.

2. Elasticity problem for semi-infinite cubic helimagnets in the skyrmion phase with a free surface

Following the unified theory of magnetoelastic effects in B20 compounds developed in [22], we write the Helmholtz free energy density for cubic helimagnets in the conventional Cartesian coordinate system O-$r_1r_2r_3$ (the cartesian axes r_1, r_2 and r_3 are collinear with the crystallographic axes) in the form

$$w = \sum_{i=1}^{3} A\left(\frac{\partial \boldsymbol{M}}{\partial r_i}\right)^2 - \boldsymbol{B}\cdot\boldsymbol{M} + b\boldsymbol{M}\cdot(\boldsymbol{\nabla}\times\boldsymbol{M}) + w_{\mathrm{an}} + w_{\mathrm{L}} + w_{\mathrm{el}} + w_{\mathrm{me}}, \tag{1}$$

where the first three terms represent respectively the Heisenberg exchange energy density with stiffness A, the Zeeman energy density with external applied magnetic field $\boldsymbol{B}$ and the DM interaction with Dzyaloshinskii constant b; $w_{\mathrm{an}} = \sum_{i=1}^{3} B_c M_i^4$ is cubic anisotropy term; $w_{\mathrm{L}} = \alpha_1(T - T_0)M^2 + \alpha_2 M^4$ are two Landau expansion terms. The last two terms in equation (1) are related to the strains. w_{el} is the elastic energy density and w_{me} the magnetoelastic energy density,

$$w_{\mathrm{el}} = \frac{1}{2}C_{11}(\varepsilon_{11}^2 + \varepsilon_{22}^2 + \varepsilon_{33}^2) + C_{12}(\varepsilon_{11}\varepsilon_{22} + \varepsilon_{11}\varepsilon_{33} + \varepsilon_{22}\varepsilon_{33}) + \frac{1}{2}C_{44}(\gamma_{12}^2 + \gamma_{13}^2 + \gamma_{23}^2), \tag{2}$$

$$\begin{aligned} w_{\mathrm{me}} = \frac{1}{M_s^2}[&L_1(M_1^2\varepsilon_{11} + M_2^2\varepsilon_{22} + M_3^2\varepsilon_{33}) \\ &+ L_2(M_3^2\varepsilon_{11} + M_1^2\varepsilon_{22} + M_2^2\varepsilon_{33}) \\ &+ L_3(M_1M_2\gamma_{12} + M_1M_3\gamma_{13} + M_2M_3\gamma_{23}) \\ &+ KM^2\varepsilon_{ii} + \sum_{i=1}^{6} L_{Oi}f_{Oi}], \end{aligned} \tag{3}$$

where $\gamma_{ij} = 2\varepsilon_{ij}$ $(i,j = 1,2,3$ and $i \neq j)$ are the engineering shear strains, ε_{ij} $(i,j = 1,2,3)$ are the strains, C_{11}, C_{22} and C_{44} are the elastic constants for cubic crystals, M_s is the saturation magnetization, M_i $(i = 1,2,3)$ are the magnetization components satisfying $M^2 = M_1^2 + M_2^2 + M_3^2$, L_i $(i = 1,2,3)$ and L_{Oi} $(i = 1,...,6)$ are magnetoelastic coupling constants and f_{Oi} $(i = 1,...,6)$ represent high order magnetoelastic coupling terms whose detailed expressions are given in [22].

In O-$r_1r_2r_3$ coordinate system, we use the triple-Q representation to approximate the magnetization field of the skyrmion lattice phase stabilized by applied magnetic field along [0 0 1] [1, 3]:

$$\boldsymbol{M}(\boldsymbol{r}) = \begin{bmatrix} 0 \\ 0 \\ \bar{M}\cos(\varphi) \end{bmatrix} + \frac{\sqrt{3}\bar{M}\sin(\varphi)}{3}\left\{ \begin{bmatrix} 0 \\ \sin(\boldsymbol{q}_1\boldsymbol{r}) \\ -\cos(\boldsymbol{q}_1\boldsymbol{r}) \end{bmatrix} + \begin{bmatrix} -\frac{\sqrt{3}}{2}\sin(\boldsymbol{q}_2\boldsymbol{r}) \\ -\frac{1}{2}\sin(\boldsymbol{q}_2\boldsymbol{r}) \\ -\cos(\boldsymbol{q}_2\boldsymbol{r}) \end{bmatrix} + \begin{bmatrix} \frac{\sqrt{3}}{2}\sin(\boldsymbol{q}_3\boldsymbol{r}) \\ -\frac{1}{2}\sin(\boldsymbol{q}_3\boldsymbol{r}) \\ -\cos(\boldsymbol{q}_3\boldsymbol{r}) \end{bmatrix} \right\}, \tag{4}$$

where $\bar{M}$ satisfies $\bar{M}^2 = \frac{1}{V}\int M^2 \mathrm{d}V$ with V the volume of a skyrmion lattice, $\tan(\varphi)$ describes the ratio of the periodic part to the averaged part of the magnetization, $\boldsymbol{q}_1 = q[1,0,0]^T$, $\boldsymbol{q}_2 = q[-\frac{1}{2}, \frac{\sqrt{3}}{2}, 0]^T$, $\boldsymbol{q}_3 = -\boldsymbol{q}_1 - \boldsymbol{q}_2$ are wavevectors with magnitude q.

For a bulk cubic crystal free from body forces and surface constrains, the incompatible eigenstrains induced by skyrmions leads to eigenstresses. In a semi-infinitely extended material (illustrated in figure B1) with eigenstresses induced by skyrmions, to set the surface boundary $z = 0$ stress-free, equal and opposite surface force should be applied, the force needed has the components

$$\begin{bmatrix} F_1 \\ F_2 \\ F_3 \end{bmatrix} = -\begin{bmatrix} \sigma_{11} & \sigma_{12} & \sigma_{13} \\ \sigma_{21} & \sigma_{22} & \sigma_{23} \\ \sigma_{31} & \sigma_{32} & \sigma_{33} \end{bmatrix}\begin{bmatrix} 0 \\ 0 \\ 1 \end{bmatrix} = -\begin{bmatrix} \sigma_{13} \\ \sigma_{23} \\ \sigma_{33} \end{bmatrix}. \tag{5}$$

Due to the superposition of three triple-Q structures of the elastic field, σ_{i3} $(i = 1,2,3)$ can be expressed in the following form

$$\sigma_{i3} = \sum_{j=1}^{3} \sigma_{i3}^{Sj}, \tag{6}$$

where the analytical expressions of the eigenstress components σ_{i3}^{Sj}, $(i,j = 1,2,3)$ are derived as equations (A.5)–(A.13) in appendix A.

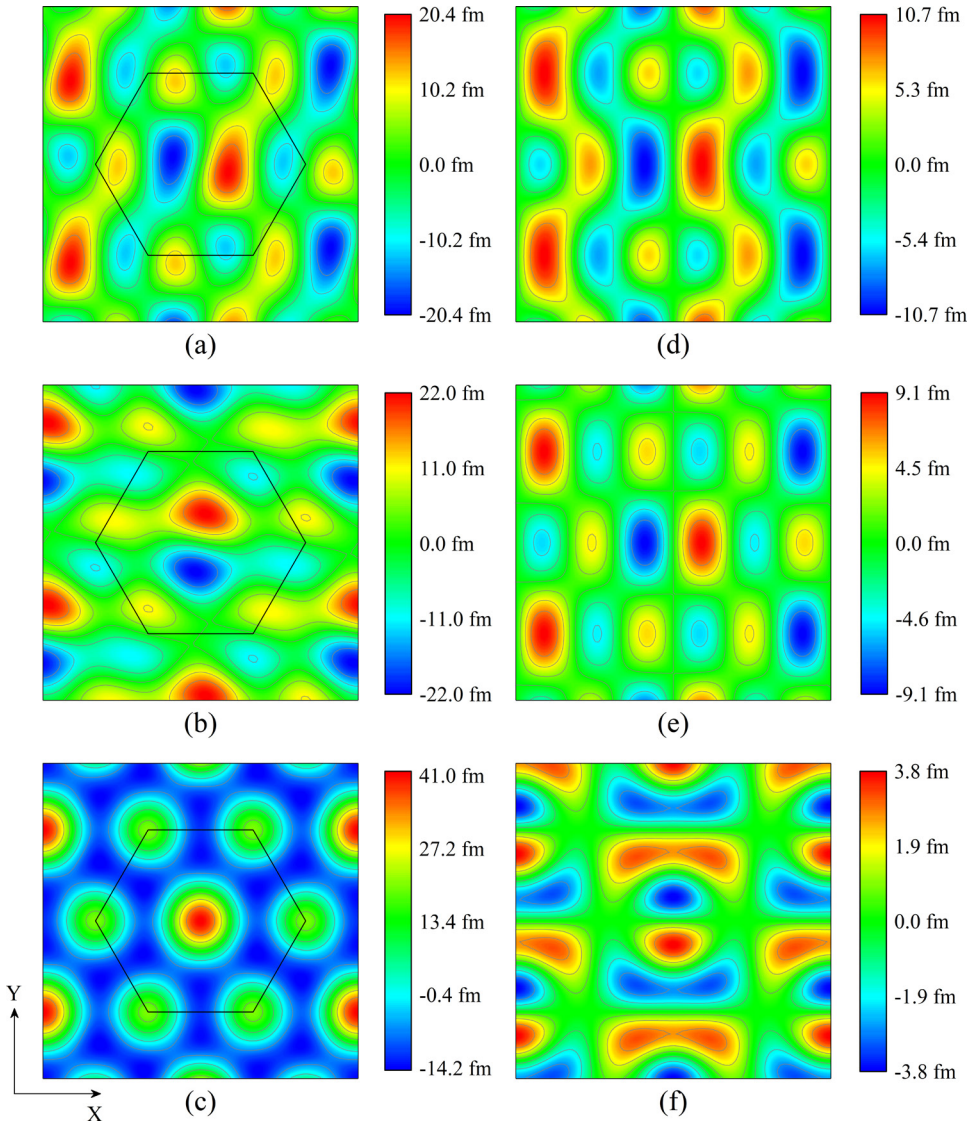

Figure 1. Contour plots of displacement components at 20 K and 0.1 T. The region enclosed by the hexagon represents a skyrmion lattice. (a)–(c) Stand for the total displacements along r_1, r_2 and r_3-direction u_1^t, u_2^t and u_3^t; (d)–(f) show the skyrmion-induced, normal-force-induced and shear-force-induced r_1-direction displacements u_1^{sky}, u_1^{nor} and u_1^{she}.

We would like to stress that σ_{33}^{S1}, whose sign is determined by φ, undergoes a 'configurational reversal' [22]; while, σ_{33}^{S3}, which is linear with respect to $\sin^2(\varphi)$, is almost constant when the applied magnetic field changes.

3. Analytical solution of surface-induced displacement field for skyrmion phase

In the coordinate system O-xyz (see figure B1) which is generated by rotating O-$r_1r_2r_3$ system around r_3-axis by θ, the surface forces $Q(x)$ (with distribution along x-axis and with direction along x-axis) and $P(x)$ (with distribution along x-axis and with direction along z-axis) cause 2D elasticity problems which are solved in appendix B, while the surface force $R(x)$ (with distribution along x-axis and with direction along y-axis) causes a 3D elasticity problem. For the 2D force distribution $Q(x) = F\cos(ax)$, the displacement field is derived as

$$u_1(x,z) = \frac{F}{a} f_{1,\theta}(z)\sin(ax),$$
$$u_3(x,z) = \frac{F}{a} f_{2,\theta}(z)\cos(ax), \tag{7}$$

where

$$f_{1,\theta}(z) = \{S_{11}\beta^2[\cos(a_1 z) + \sqrt{\frac{1+\mu'}{1-\mu'}}\sin(a_1 z)] + S_{13}[\cos(a_1 z) - \sqrt{\frac{1+\mu'}{1-\mu'}}\sin(a_1 z)]\}\mathrm{e}^{a_2 z},$$
$$f_{2,\theta}(z) = \sqrt{2(1+\mu')}\{\frac{S_{31}\beta}{\sqrt{1-\mu'^2}}\sin(a_1 z) + \frac{S_{33}}{\beta}[\cos(a_1 z) - \frac{\mu'}{\sqrt{1-\mu'^2}}\sin(a_1 z)]\}\mathrm{e}^{a_2 z}. \tag{8}$$

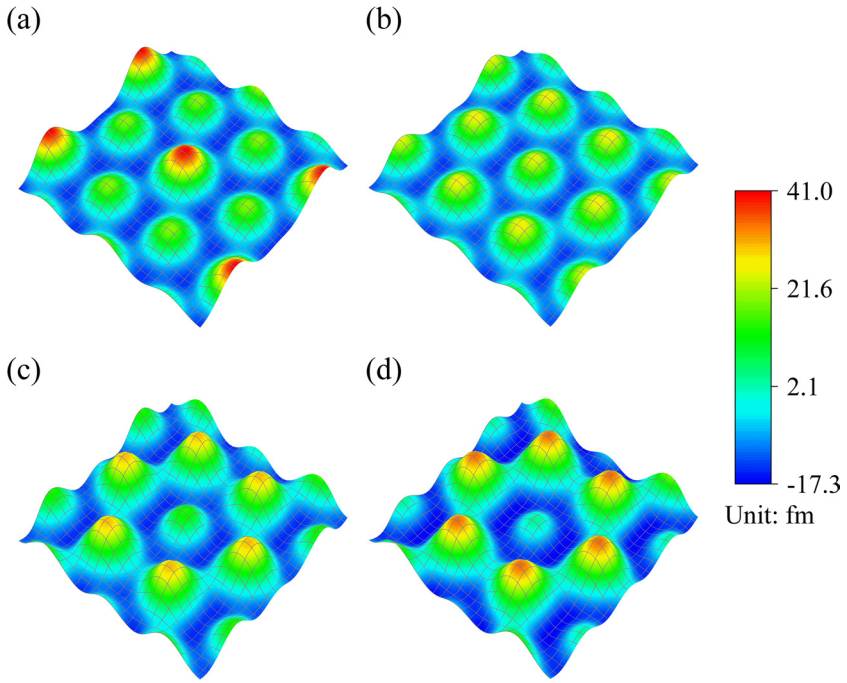

Figure 2. Surface configuration (u_3) for MnSi in skyrmion phase at temperature 20 K and magnetic field (a) 0.1 T, (b) 0.175 T, (c) 0.225 T and (d) 0.275 T. The size of (a)–(d) is $\frac{2\pi}{q} \times \frac{2\pi}{q}$.

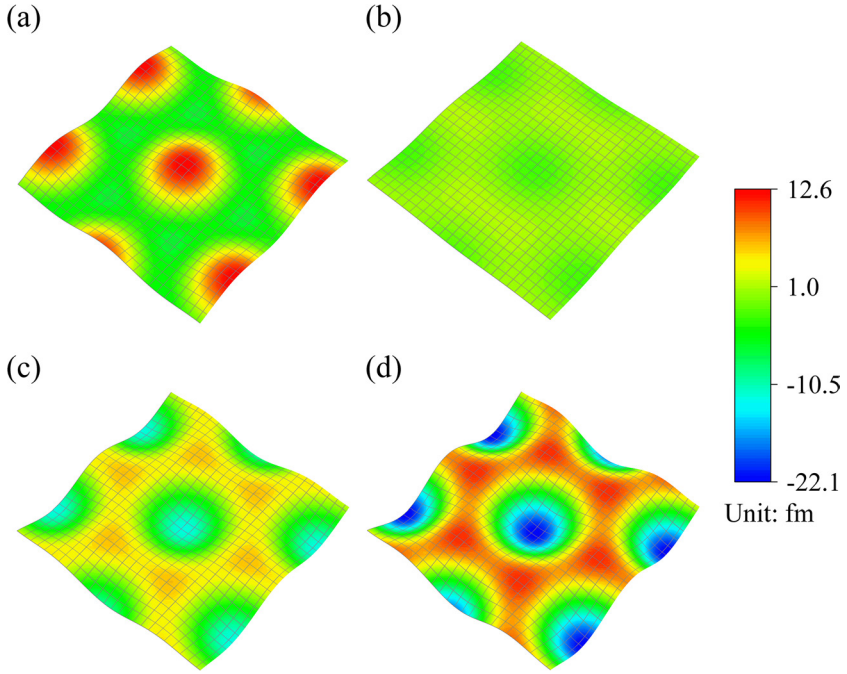

Figure 3. Reversible surface configuration of u_3^{s1} for MnSi in skyrmion phase at temperature 20 K and magnetic field (a) 0.1 T, (b) 0.175 T, (c) 0.225 T and (d) 0.275 T.

S_{ij}, β and μ', whose expressions can be found in appendix B, are related to θ, $a_1 = \sqrt{\frac{1-\mu'}{2}}\beta a$ and $a_1 = \sqrt{\frac{1+\mu'}{2}}\beta a$.

The displacement field is composed of two parts: one is the harmonic term having the same period as the force distribution, the other is the z-related term having an exponential factor $e^{a_2 z}$. $a_2 = \sqrt{\frac{1+\mu'}{2}}\beta a$ is positive; therefore, the displacement decreases rapidly with decreasing z. When the distance from the boundary is greater than several times of wavelength of the harmonic force distribution, the displacement is negligible. Thus, the elastic field derived in [12] is suitable for bulk materials.

Similarly, for $P(x) = F\sin(ax)$, we can derive the displacement field as:

$$u_1(x,z) = \frac{F}{a} f_{3,\theta}(z)\sin(ax),$$
$$u_3(x,z) = \frac{F}{a} f_{4,\theta}(z)\cos(ax), \tag{9}$$

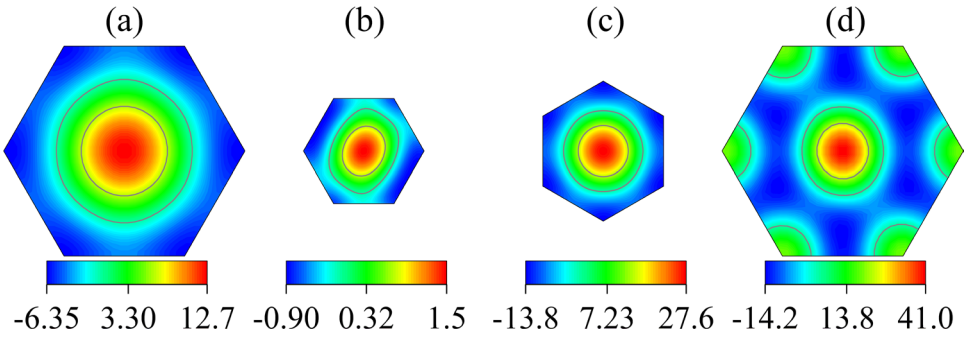

Figure 4. The simplest repeating unit of surface displacement (the unit is fm). (a) u_3^{Q1}, (b) u_3^{Q2}, (c) u_3^{Q3} and (d) u_3 for MnSi in skyrmion phase at 20 K and 0.1 T.

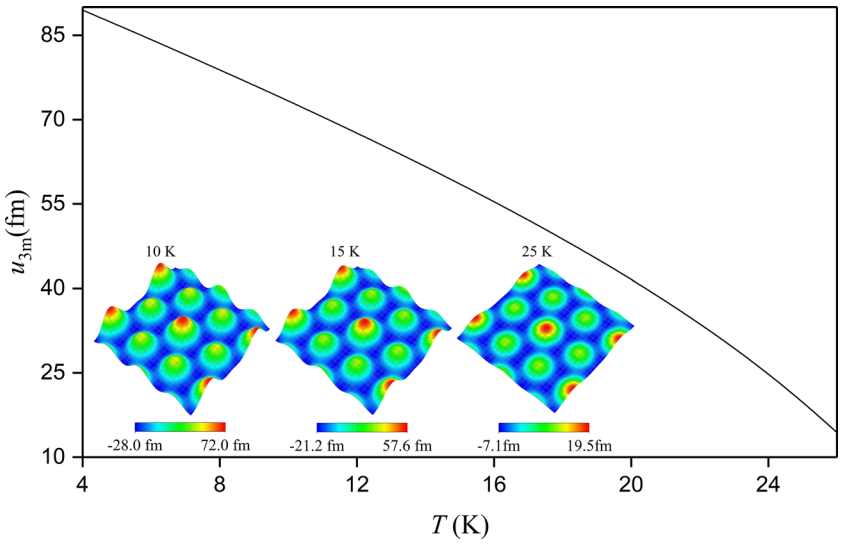

Figure 5. Maximum displacement along z-axis as a funciton of temperature at 0.1 T. Insets show the surface configurations at magnetic field 0.1 T and temperature 10 K, 15 K and 25 K.

where

$$f_{3,\theta}(z) = \sqrt{2(1+\mu')}\{-\frac{S_{13}}{\sqrt{1-\mu'^2}}\sin(a_1 z) + S_{11}\beta^2[\cos(a_1 z) + \frac{\mu'}{\sqrt{1-\mu'^2}}\sin(a_1 z)]\}e^{a_2 z},$$

$$f_{4,\theta}(z) = \{S_{31}\beta[\cos(a_1 z) + \sqrt{\frac{1+\mu'}{1-\mu'}}\sin(a_1 z)] + \frac{S_{33}}{\beta}[\cos(a_1 z) - \sqrt{\frac{1+\mu'}{1-\mu'}}\sin(a_1 z)]\}e^{a_2 z}. \quad (10)$$

For $R(x) = F\sin(ax)$, we search for the displacement solution in the following form

$$u_1 = u_3 = 0,\ u_2(x,z) = \frac{F}{a}f_{5,\theta}(z)\sin(ax). \quad (11)$$

Here, $f_{5,\theta}(z) = S_{44}e^{az}$.

The r_1, r_2 and r_3-direction forces $F_1 = -\sigma_{13}$, $F_2 = -\sigma_{23}$ and $F_3 = -\sigma_{33}$ are composed of nine $\boldsymbol{q}_{ij}$ (see equation (A.3)) structures. For each $\boldsymbol{q}_{ij}$ structure of F_1 or F_2, the components in the direction of and perpendicular to $\boldsymbol{q}_{ij}$ are P-type and R-type forces, respectively. For $\boldsymbol{q}_{ij}$ structures of F_3, they are Q-type forces. Solving the displacement field for each $\boldsymbol{q}_{ij}$ structure in corresponding O-xyz system and projecting it onto the r_1, r_2 and r_3-axes, we can finally get the surface-induced displacement field in O-$r_1r_2r_3$ system as in equations (12), where f_k^{ij} $(k = 1, ..., 5)$ takes the value of $f_{k,\theta}(0)$ for $\theta = \arccos\left(\frac{\boldsymbol{e}_1\cdot\boldsymbol{q}_{ij}}{|\boldsymbol{q}_{ij}|}\right)$, $\boldsymbol{e}_1$, $\boldsymbol{e}_2$ and $\boldsymbol{e}_3$ are the unit vectors along r_1, r_2 and r_3-axis respectively, i is the imaginary unit. The analytical solution given by equations (12) is derived upon the triple-Q representation of magnetization. For higher order Fourier representation of magnetization, the solution of u_i takes a form similar to that given in equations (12), where the summation upper limit of i and j is more than 3. According to previous studies in terms of the Fourier representation [1, 3], the magnitudes of Fourier components of $\boldsymbol{M}$ decrease sharply with the expansion order. The solution given in equations (12) provides an effective description of the surface configuration of skyrmion lattices.

$$u_1 = -\sum_{i,j,k=1}^{3}\left(\frac{f_1^{ij}(\boldsymbol{e}_1\cdot\boldsymbol{q}_{ij})}{|\boldsymbol{q}_{ij}|^2}+\frac{f_3^{ij}(\boldsymbol{e}_k\cdot\boldsymbol{q}_{ij})\,(\boldsymbol{e}_1\cdot\boldsymbol{q}_{ij})}{|\boldsymbol{q}_{ij}|^3}\mathrm{i}+\frac{f_5^{ij}((\boldsymbol{q}_{ij}\times\boldsymbol{e}_k)\cdot\boldsymbol{e}_3)((\boldsymbol{q}_{ij}\times\boldsymbol{e}_1)\cdot\boldsymbol{e}_3)}{|\boldsymbol{q}_{ij}|^3}\mathrm{i}\right)\sigma_{k3}^{Sij}\sin(\boldsymbol{r}\cdot\boldsymbol{q}_{ij}),$$

$$u_2 = -\sum_{i,j,k=1}^{3}\left(\frac{f_1^{ij}(\boldsymbol{e}_2\cdot\boldsymbol{q}_{ij})}{|\boldsymbol{q}_{ij}|^2}+\frac{f_3^{ij}(\boldsymbol{e}_k\cdot\boldsymbol{q}_{ij})\,(\boldsymbol{e}_2\cdot\boldsymbol{q}_{ij})}{|\boldsymbol{q}_{ij}|^3}\mathrm{i}+\frac{f_5^{ij}((\boldsymbol{q}_{ij}\times\boldsymbol{e}_k)\cdot\boldsymbol{e}_3)((\boldsymbol{q}_{ij}\times\boldsymbol{e}_2)\cdot\boldsymbol{e}_3)}{|\boldsymbol{q}_{ij}|^3}\mathrm{i}\right)\sigma_{k3}^{Sij}\sin(\boldsymbol{r}\cdot\boldsymbol{q}_{ij}),$$

$$u_3 = -\sum_{i,j,k=1}^{3}\left(\frac{f_2^{ij}(\boldsymbol{e}_k\cdot\boldsymbol{e}_3)}{|\boldsymbol{q}_{ij}|}+\frac{f_4^{ij}(\boldsymbol{e}_k\cdot\boldsymbol{q}_{ij})}{|\boldsymbol{q}_{ij}|}\mathrm{i}\right)\sigma_{k3}^{Sij}\cos(\boldsymbol{r}\cdot\boldsymbol{q}_{ij}). \tag{12}$$

4. Discussion

4.1. Tunability of surface configuration by bias magnetic field

For helimagnet MnSi, the related parameters are: $C_{11} = 2.83\times10^{11}$ Pa, $C_{12} = 0.641\times10^{11}$ Pa, $C_{44} = 1.179\times10^{11}$ Pa [23], $K = -2\times10^{7}$ JA^{-2} m^{-1}, $L_1 = -0.7\times10^{6}$ JA^{-2} m^{-1}, $L_2 = 0.6\times10^{6}$ JA^{-2} m^{-1}, $L_3 = 1.646\times10^{6}$ JA^{-2} m^{-1}, $L_{O1} = 1.147\times10^{-4}$ JA^{-2}m^{-2}, $L_{O2} = -0.537\times10^{-4}$ JA^{-2} m^{-2}, $L_{O3} = -0.537\times10^{-4}$ JA^{-2}m^{-2}, $L_{O4} = L_{O5} = L_{O6} = 0$ [24], and $q = \frac{|b|}{2A} = 4.5\times10^{8}$ m^{-1} [1, 25]. According to the analytical expressions of surface-induced displacement field in equations (12) and skyrmion-induced displacement field in [40], the contour maps of the displacement components at 20 K and 0.1 T are plotted in figure 1. At the center and the six vertexes of a skyrmion lattice, there appear the peaks, for which the r_1 and r_2-components of the total displacement, u_1^t and u_2^t, are zero; while the r_3-component, u_3^t, takes a maximum value. At the right-hand part and upper part of a peak, we have $u_1^t > 0$ and $u_2^t > 0$, respectively; this indicates the tendency of expansion of the peaks. u_1^t and u_2^t are a little deformed. To explain this, the skyrmion-induced, normal-force-induced and shear-force-induced r_1-direction displacements u_1^{sky}, u_1^{nor} and u_1^{she} are plotted in figures 1(d)–(f), respectively. u_1^{sky} and u_1^{nor} share the same pattern with zero-value contour lines along r_2-axis; while u_1^{she} shows different behavior with zero-value contour lines along r_1-axis. It is the shear force who causes the deformation of u_1^{sky}. The surface configuration is determined by u_1, u_2 and u_3, but in fact, the height change of each point at the surface caused by u_1 and u_2 can be demonstrated less than 0.164 fm which is 0.4% of the maximum height 41 fm. Therefore, u_3 dominates the surface configuration.

We plot the surface configuration (u_3) of skyrmions at 20 K and under different applied magnetic field B. Figures 2(a)–(d) represent the total normal surface displacement field at 0.1 T, 0.175 T, 0.225 T and 0.275 T respectively. At 0.175 T, the surface is characterized by peaks (arranged periodically like the triangular skyrmion lattices) with almost the same height . For $B > 0.175$ T, the center peak is higher than the six adjacent peaks, while for $B < 0.175$ T, the reverse is the case, indicating that the heights of these two types of peaks compete with each other.

To explain the competing behavior of these two patterns of peaks, we explore separately the two dominant parts of the displacement: the σ_{33}^{S1}-induced normal displacement u_3^{s1} and the σ_{33}^{S3}-induced normal displacement u_3^{s3}. Figure 3 shows the surface displacement u_3^{s1} at 0.1 T, 0.175 T, 0.225 T and 0.275 T. It can be seen that u_3^{s1} goes through the same 'configurational reversal' as σ_{33}^{S1} when the external magnetic field increases. At 0.1 T, there are periodically arranged peaks on the surface. With the augmentation of the magnetic field, the height of the peaks decreases, then at about 0.175 T, when $\tan(\varphi) \approx 2.31$, the peaks vanishes, and the surface described by u_3^{s1} becomes almost flat. For $B > 0.175$ T, on the surface, there appears the valleys, the depth of which increases when the magnetic field augments. The 'configurational reversal' can be explained through the relation between u_3^{s1} and σ_{33}^{S1} revealed by equations (12). As for u_3^{s3}, equations (12) and the invariability of σ_{33}^{S3} imply that u_3^{s3} keeps almost unchanged when magnetic field changes. It is the reversal feature of u_3^{s1} and the invariability of u_3^{s3} that decide the competing behavior of two patterns of peaks.

According to equations (12), the displacement field u_3 can be divided into three triple-Q structures: u_3^{Q1}, u_3^{Q2} and u_3^{Q3}, corresponding to $\boldsymbol{q}_{1i}$, $\boldsymbol{q}_{2i}$ and $\boldsymbol{q}_{3i}$ $(i = 1, 2, 3)$, respectively. To explore the periodicity of u_3, we plot the simplest repeating unit of surface displacement u_3^{Q1}, u_3^{Q2}, u_3^{Q3} and u_3 at 20 K and 0.1 T in figure 4. We can see that u_3^{Q1} and u_3 share the same periodicity. The primitive vectors for the hexagonal lattices of u_3^{Qi} are $\boldsymbol{a}_{i1}$ and $\boldsymbol{a}_{i2}$, satisfying $\boldsymbol{a}_{ij}\cdot\boldsymbol{q}_{ik} = 2\pi\delta_{jk}$ where $i = 1, 2, 3$ and $j, k = 1, 2$, δ_{jk} is the Kronecker delta. We can demonstrate that $\boldsymbol{a}_{11} = 2\boldsymbol{a}_{21} = \boldsymbol{a}_{31} + 2\boldsymbol{a}_{32}$ and $\boldsymbol{a}_{12} = 2\boldsymbol{a}_{22} = -\boldsymbol{a}_{31} + \boldsymbol{a}_{32}$. Thus, for arbitrary integers n_1 and n_2, we have $u_3^{Q2}(\boldsymbol{r} + n_1\boldsymbol{a}_{11} + n_2\boldsymbol{a}_{12}) = u_3^{Q3}(\boldsymbol{r} + 2(n_1+n_2)\boldsymbol{a}_{21} + 2(n_1+n_2)\boldsymbol{a}_{22}) = u_3^{Q2}(\boldsymbol{r})$ and $u_3^{Q3}(\boldsymbol{r} + n_1\boldsymbol{a}_{11} + n_2\boldsymbol{a}_{12}) = u_3^{Q3}(\boldsymbol{r} + (n_1 - n_2)\boldsymbol{a}_{31} + (2n_1 + n_2)\boldsymbol{a}_{32}) = u_3^{Q3}(\boldsymbol{r})$. Consequently, u_3 has the same period as u_3^{Q1} and the skyrmion lattices. By using the relations between $\boldsymbol{a}_{ij}$, u_1 and u_2 can also be demonstrated to share the same periodicity as the skyrmion lattices.

The magnitude of magnetization changes with temperature, for which the amplitude of surface configuration is also affected. Figure 5 shows the maximum displacement along z-axis as a function of temperature at 0.1 T, while in the insets the surface configurations at three different temperature points are plotted. With increasing (decreasing) temperature, the shape of surface configuration merely changes, but the amplitude decreases (increases). When the magnetization is saturated,

the maximum displacement is about 89.5 fm. It should also be mentioned that, at different temperature, the corresponding u_3^{s1} still undergoes the 'configurational reversal' with increasing magnetic field.

4.2. Possible effects of electric current and mechanical load on the surface configuration

It is known that skyrmions behave like moving particles with stable topological structures when exposed to various kinds of external fields including electric current [11, 26] and temperature gradient [27]. A further concern is how will the surface configuration change with the motion of skyrmions. For moving skyrmions at speed $\boldsymbol{v}$, the magnetization can be described by introducing a translation transformation: $\boldsymbol{r} \to \boldsymbol{r} - \boldsymbol{v}t$. Thus, we have $\boldsymbol{M} = \boldsymbol{M}(\boldsymbol{r} - \boldsymbol{v}t)$, where $\boldsymbol{M}(\boldsymbol{r})$ is expressed as equation (4). Correspondingly, the solution of u_i $(i = 1, 2, 3)$ obtained in equations (12) is changed by replacing $\boldsymbol{r}$ with $\boldsymbol{r} - \boldsymbol{v}t$, i.e. $u_i = u_i(\boldsymbol{r} - \boldsymbol{v}t)$. Thus, the displacement field moves together with skyrmions.

When anisotropic mechanical loads are applied to helimagnets, skyrmion lattices are found to undergo emergent elastic deformation independent of the deformation of the underlying atomic lattices [21]. It is shown in [28] that the deformed skyrmions have a triple-Q structure characterized by $\boldsymbol{q}_1$, $\boldsymbol{q}_2$ and $\boldsymbol{q}_3$ satisfying $|\boldsymbol{q}_1| \neq |\boldsymbol{q}_2| \neq |\boldsymbol{q}_3|$ and $\boldsymbol{q}_1 + \boldsymbol{q}_2 + \boldsymbol{q}_3 = \boldsymbol{0}$. For a general analysis, we can see that the periodic eigenstrains obtained from equation (A.1) is still composed of three triple-Q structures. The periodic stress field, linearly related to the incompatible part of eigenstrains, obviously shares the same periodicity with the eigenstrains. From equations (12), we can see that for arbitrarily deformed skyrmion lattices, u_3^{Q1} and u_3^{Q2} has the same periodicity with the deformed skyrmions, while u_3^{Q3} is a triple-Q structure with the three 'Q's: $\boldsymbol{q}_1 - \boldsymbol{q}_2, \boldsymbol{q}_1 - \boldsymbol{q}_3$ and $\boldsymbol{q}_2 - \boldsymbol{q}_3$. Following the proof of the periodicity given in this section, we can easily show that u_3^{Q3} and u_3 share the same periodicity, because $\boldsymbol{q}_1 + \boldsymbol{q}_2 + \boldsymbol{q}_3 = \boldsymbol{0}$ is the only necessary condition which is still valid for any deformed skyrmion lattices. Therefore, the surface displacement field deforms together with the skyrmion lattices.

We have proved qualitatively that the surface displacement field moves together, and deforms together with the skyrmion lattices. Therefore, the various kinds of approaches discovered to affect the skyrmion lattices will also be effective in controlling the surface displacement field.

4.3. Generality and possible technological interest.

Apart from 2D DM-induced Bloch-type magnetic skyrmion lattices in helimagnets, skyrmions can exist in many other forms: 3D skyrmions, such as hourglass-shaped skyrmions [29] and bobber-shaped skyrmions [30]; atomic-scale skyrmions induced by four-spin interaction [31], skyrmion bubbles induced by spin–orbit interaction [32, 33]and stabilized by uniaxial anisotropy [34, 35]; Néel-type skyrmions [36]; isolated skyrmion and skyrmion glass structure [17]. Since magnetoelastic coupling is intrinsic for any ferromagnets, these skyrmions forms are all accompanied by a surface displacement field. Thus, the surface configuration is an additional particle-like property of any magnetic skyrmions.

The maximum displacement perpendicular to the surface is of the order of magnitude of 10^{-13} m for MnSi. Such a small displacement is difficult to detect. But as shown in formulae (A.5)–(A.13), and (12), the displacement is related to the magnetoelastic coefficients, and the size of skyrmion lattices. To get a greater displacement, one should pay attention to materials hosting skyrmions with bigger size and having stronger magnetoelastic coupling, for instance, FeGe. Even though the magnetoelastic coefficients are not available due to the technical difficulties in fabricating large FeGe single crystals [37], one can expect to observe larger displacement field for FeGe than for MnSi. The skyrmion lattice parameter for FeGe is about 70 nm [38], four times larger than that for MnSi. Moreover, the experiment carried out by Shibata *et al* [21], in which anisotropic strain as small as 0.3% induced distortions of skyrmion lattices by 20%, implies large magnetoelastic coupling in FeGe.

5. Conclusions

To conclude, we have obtained the analytical solution of displacement field at the surface of cubic helimagnets in skyrmion phase dominated by u_3. For MnSi, the normal displacement field is dominated by two triple-Q structures u_3^{s1} and u_3^{s3}. u_3^{s3} is characterized by periodically arranged peaks having invariant height when applied magnetic field changes and u_3^{s1}, undergoing a 'configurational reversal' when the magnetic field increases from 0.1 T to 0.275 T, distinguishes these peaks into two patterns which compete with each other. The surface configuration enriches the meaning of particle-like nature of magnetic skyrmions, it moves and deforms with the skyrmions lattices and can be therefore controlled by applied field, such as magnetic field, current etc.

Acknowledgments

The work was supported by the NSFC (National Natural Science Foundation of China) through the funds 11772360, 11302267, 11472313, 11572355 and Pearl River Nova Program of Guangzhou (Grant No. 201806010134).

Appendix A. Analytical solution of the skyrmion-induced stress field

For a bulk cubic crystal free from body forces and surface constraints, we obtain the expressions of eigenstrains $\varepsilon_{ij}^* = \varepsilon_{ij}^*(\boldsymbol{M})$ $(i,j = 1,2,3)$ by solving the equations $\sigma_{IJ}(\varepsilon_{ij}^*, \boldsymbol{M}) = 0$ $(I,J,i,j = 1,2,3)$, where σ_{IJ}, a function of $\varepsilon_{ij}(i,j = 1,2,3)$ and $\boldsymbol{M}$, is obtained by $\sigma_{IJ}(\varepsilon_{ij}, \boldsymbol{M}) = \frac{\partial w}{\partial \varepsilon_{IJ}}$ (for $I = J$) and $\sigma_{IJ}(\varepsilon_{ij}, \boldsymbol{M}) = \frac{\partial w}{\partial \gamma_{IJ}}$ (for $I \neq J$).

$$
\begin{aligned}
\varepsilon^*_{11} &= K^*M^2 - L^*_1M^2_1 - L^*_2M^2_3 + L^*_{O1}(M_3M_{1,2} - M_2M_{1,3}) + L^*_{O2}(M_3M_{2,1} - M_2M_{3,1}) + L^*_{O3}M_1(M_{2,3} - M_{3,2}),\\
\varepsilon^*_{22} &= K^*M^2 - L^*_1M^2_2 - L^*_2M^2_1 + L^*_{O1}(M_1M_{2,3} - M_3M_{2,1}) + L^*_{O2}(M_1M_{3,2} - M_3M_{1,2}) + L^*_{O3}M_2(M_{3,1} - M_{1,3}),\\
\varepsilon^*_{33} &= K^*M^2 - L^*_1M^2_3 - L^*_2M^2_2 + L^*_{O1}(M_2M_{3,1} - M_1M_{3,2}) + L^*_{O2}(M_2M_{1,3} - M_1M_{2,3}) + L^*_{O3}M_3(M_{1,2} - M_{2,1}),\\
\gamma^*_{2,3} &= \frac{1}{C_{44}M^2_s}\left[-L_3M_2M_3 + L_{O6}M_1(M_{2,2} - M_{3,3}) + M_2(L_{O4}M_{1,2} + L_{O5}M_{2,1}) - M_3(L_{O4}M_{1,3} + L_{O5}M_{3,1})\right],\\
\gamma^*_{1,3} &= \frac{1}{C_{44}M^2_s}\left[-L_3M_1M_3 + L_{O6}M_2(M_{3,3} - M_{1,1}) + M_3(L_{O4}M_{2,3} + L_{O5}M_{3,2}) - M_1(L_{O4}M_{2,1} + L_{O5}M_{1,2})\right],\\
\gamma^*_{1,2} &= \frac{1}{C_{44}M^2_s}\left[-L_3M_1M_2 + L_{O6}M_3(M_{1,1} - M_{2,2}) + M_1(L_{O4}M_{3,1} + L_{O5}M_{1,3}) - M_2(L_{O4}M_{3,2} + L_{O5}M_{2,3})\right],
\end{aligned}
\tag{A.1}
$$

with $K^* = \frac{-C_{11}K + C_{12}(K+L_1+L_2)}{(C_{11}-C_{12})(C_{11}+2C_{12})M^2_s}$, $L^*_1 = \frac{L_1}{(C_{11}-C_{12})M^2_s}$, $L^*_2 = \frac{L_2}{(C_{11}-C_{12})M^2_s}$, $L^*_{O1} = \frac{-C_{11}L_{O1} + C_{12}(-L_{O1}+L_{O2}+L_{O3})}{(C_{11}-C_{12})(C_{11}+2C_{12})M^2_s}$, $L^*_{O2} = \frac{C_{11}L_{O2} - C_{12}(-L_{O1}+L_{O2}+L_{O3})}{(C_{11}-C_{12})(C_{11}+2C_{12})M^2_s}$ and $L^*_{O3} = \frac{C_{12}(L_{O1}+L_{O2}) - (C_{11}+C_{12})L_{O3}}{(C_{11}-C_{12})(C_{11}+2C_{12})M^2_s}$.

By substituting the Hooke's law and the geometrical equations $\varepsilon_{ij} = \frac{u_{i,j}+u_{j,i}}{2}$ into the equilibrium equations, we obtain three partial differential equations about the displacements u_i

$$
\begin{aligned}
&C_{11}u_{i,ii} + C_{44}(u_{i,jj} + u_{i,kk}) + (C_{12} + C_{44})(u_{j,ij} + u_{k,ik})\\
&= C_{11}\varepsilon^*_{ii,i} + C_{12}(\varepsilon^*_{jj,i} + \varepsilon^*_{kk,i}) + C_{44}(\gamma^*_{ij,j} + \gamma^*_{1k,k}),
\end{aligned}
\tag{A.2}
$$

where $i,j,k = 1,2,3$ and $i \neq j \neq k$.

$\varepsilon^*_{ij} = \varepsilon^*_{ij}(\boldsymbol{M})$ and $\gamma^*_{ij} = \gamma^*_{ij}(\boldsymbol{M})$ are quadratic functions of $\boldsymbol{M}$ [22]. By substituting the triple-Q periodic form of $\boldsymbol{M}$ into the obtained eigenstrains, we can find that eigenstrains have a multi-Q structure with nine wavevectors $\boldsymbol{q}_{ij}$ $(i,j = 1,2,3)$ defined as:

$$
[\boldsymbol{q}_{ij}] = \begin{bmatrix} \boldsymbol{q}_1 & \boldsymbol{q}_2 & \boldsymbol{q}_3 \\ 2\boldsymbol{q}_1 & 2\boldsymbol{q}_2 & 2\boldsymbol{q}_3 \\ \boldsymbol{q}_1 - \boldsymbol{q}_2 & \boldsymbol{q}_1 - \boldsymbol{q}_3 & \boldsymbol{q}_2 - \boldsymbol{q}_3 \end{bmatrix}. \tag{A.3}
$$

This multi-Q structure can be seen as the superposition of three triple-Q structures with different magnitudes q, $2q$ and $\sqrt{3}q$. Combining the geometrical equations, eigenstrains and Hooke's law, we then derive the triple-Q structure stresses as :

$$
\sigma^{Sk}_{ij} = \mathrm{Re}\left[\sum_{l=1}^{3} \sigma^{Skl}_{ij} \mathrm{e}^{\mathrm{i}\boldsymbol{q}_{kl}\cdot\boldsymbol{r}}\right] \quad (i,j,k = 1,2,3) \tag{A.4}
$$

where

$$
\begin{bmatrix} \sigma^{S11}_{13} \\ \sigma^{S12}_{13} \\ \sigma^{S13}_{13} \end{bmatrix} = \frac{\mathrm{i}L_3\bar{M}^2}{12M^2_s}\sin(\varphi)(6\cos(\varphi) - \sqrt{3}\sin(\varphi)) \begin{bmatrix} 0 \\ 1 \\ -1 \end{bmatrix}, \tag{A.5}
$$

$$
\begin{bmatrix} \sigma^{S21}_{13} \\ \sigma^{S22}_{13} \\ \sigma^{S23}_{13} \end{bmatrix} = -\frac{\mathrm{i}L_3\bar{M}^2}{4\sqrt{3}M^2_s}\sin^2(\varphi) \begin{bmatrix} 0 \\ 1 \\ -1 \end{bmatrix}, \tag{A.6}
$$

$$
\begin{bmatrix} \sigma^{S31}_{13} \\ \sigma^{S32}_{13} \\ \sigma^{S33}_{13} \end{bmatrix} = \frac{\mathrm{i}L_3\bar{M}^2}{4\sqrt{3}M^2_s}\sin^2(\varphi) \begin{bmatrix} 1 \\ -1 \\ -2 \end{bmatrix}, \tag{A.7}
$$

$$
\begin{bmatrix} \sigma^{S11}_{23} \\ \sigma^{S12}_{23} \\ \sigma^{S13}_{23} \end{bmatrix} = \frac{\mathrm{i}L_3\bar{M}^2}{12M^2_s}\sin(\varphi)(2\sqrt{3}\cos(\varphi) - \sin(\varphi)) \begin{bmatrix} 2 \\ -1 \\ -1 \end{bmatrix}, \tag{A.8}
$$

$$
\begin{bmatrix} \sigma^{S21}_{23} \\ \sigma^{S22}_{23} \\ \sigma^{S23}_{23} \end{bmatrix} = -\frac{\mathrm{i}L_3\bar{M}^2}{12M^2_s}\sin^2(\varphi) \begin{bmatrix} 2 \\ -1 \\ -1 \end{bmatrix}, \tag{A.9}
$$

$$
\begin{bmatrix} \sigma^{S31}_{23} \\ \sigma^{S32}_{23} \\ \sigma^{S33}_{23} \end{bmatrix} = \frac{\mathrm{i}L_3\bar{M}^2}{4M^2_s}\sin^2(\varphi) \begin{bmatrix} 1 \\ 1 \\ 0 \end{bmatrix}, \tag{A.10}
$$

$$
\begin{aligned}
\sigma^{S11}_{33} =& -\frac{\sin(\varphi)\bar{M}^2}{12M^2_sC_{11}}\{4\sqrt{3}\cos(\varphi)[-C_{12}(2K + qL_{O2} + C_{11}(2K + 2L_1 + qL_{O3})) + \sin(\varphi)[C_{11}(-6K\\
&- 4L_1 + L_2 - 2qL_{O1} - 4qL_{O3}) + C_{12}(6K + 3L_1 - 2L_2 + 3qL_{O1} + 3qL_{O3})]]\},\\
\sigma^{S12}_{33} =& \sigma^{S13}_{33} = \frac{\sin(\varphi)\bar{M}^2}{6C_kM^2_s}\{-2\sqrt{3}\cos(\varphi)[3C^2_{11}(2K + 2L_1 + qL_{O3}) - C_{11}(3C_{12}(4K - q(L_{O1} + L_{O2}))\\
&- 10C_{44}(2K + 2L_1 + qL_{O3})) + C_{12}(3C_{12}(2K - 2L_1 + q(L_{O1} + L_{O2} - L_{O3})) - 2C_{44}(10K\\
&+ 6L_1 - 12L_2 + 2qL_{O2} + 3qL_{O3}))] + \sin(\varphi)[3C^2_{11} \times (3K + 2L_1 + L_2 + qL_{O1} + 2qL_{O3}) + C_{11}(-3\\
&\times C_{12}(6K + L_1 - L_2 + 2L_3 + 2qL_{O1} + 3qL_{O2} + qL_{O3}) + 10C_{44}(3K + 2L_1 + L_2 + qL_{O1}\\
&+ 2qL_{O3})) + C_{12}(3C_{12}(3KK - L_1 - 2L_2 + 2L_3 + qL_{O1} + 3qL_{O2} - qL_{O3}) - 2C_{44}(15K + 9L_1\\
&- 14L_2 + 6qL_{O1} + 9qL_{O3}))]\},
\end{aligned}
\tag{A.11}
$$

$$\sigma_{33}^{S21} = \frac{\bar{M}^2}{6C_{11}M_s^2}\sin^2(\varphi)[-C_{12}L_2 + C_{11}(L_1 - L_2 - qL_{O1} + qL_{O3})],$$

$$\begin{aligned}\sigma_{33}^{S22} = \sigma_{33}^{S23} = \frac{\bar{M}^2}{24C_kM_s^2}\sin^2(\varphi) \times \{&3C_{11}^2(4L_1 - L_2 - 4qL_{O1} + 4qL_{O3}) \\ &+ C_{11}[-10C_{44}(-4L_1 + L_2 + 4qL_{O1} - 4qL_{O3}) + 3C_{12}(4L_1 - L_2 - 4L_3 - 4qL_{O1} + 4qL_{O3})] \\ &+ 2C_{12}[4C_{44}(-3L_1 + 4L_2 + 3qL_{O1} - 3qL_{O3}) - 3C_{12}(4L_1 - L_2 - 2L_3 - 4qL_{O1} + 4qL_{O3})]\},\end{aligned} \tag{A.12}$$

$$\begin{aligned}\sigma_{33}^{S31} = \sigma_{33}^{S32} = \frac{\sin^2(\varphi)\bar{M}^2}{6C_{11}M_s^2}\{&3C_{11}^2(K + 2L_1 - L_2 - qL_{O1} + 2qL_{O3}) - C_{11}[3C_{12}(2K - L_1 + L_2 \\ &+ 2L_3 + 2qL_{O1} + qL_{O2} - qL_{O3}) - 10C_{44}(K + 2L_1 - L_2 - qL_{O1} + 2qL_{O3})] + C_{12}[3C_{12}(K \\ &- 3L_1 + 2L_2 + 2L_3 + 3qL_{O1} + qL_{O2} - 3qL_{O3}) - 2C_{44}(5K + 7L_1 - 2L_2 - 2qL_{O1} + 7qL_{O3})]\},\end{aligned}$$

$$\begin{aligned}\sigma_{33}^{S33} = \frac{\bar{M}^2}{12C_{11}M_s^2}\sin^2(\varphi)&[-C_{12}(2K + L_1 - 5L_2 + qL_{O1} + qL_{O3}) \\ &+ C_{11}(2K + 4L_1 + L_2 - 2qL_{O1} + 4qL_{O3})],\end{aligned} \tag{A.13}$$

and $C_k = 3C_{11}^2 + 10C_{11}C_{44} - 3C_{12}(C_{12} + 2C_{44})$. Here, to simplify the formulae, we have set the high order magnetoelastic coefficients L_{O4}, L_{O5} and L_{O6} to zero.

Strictly speaking, the free energy is a functional of the magnetization $\boldsymbol{M}$ and the strains ε_{ij}. Due to the magnetoelastic coupling, the elastic fields are related to $\boldsymbol{M}$ at equilibrium state, i.e. the elastic strains $\varepsilon_{ij} = \varepsilon_{ij}(\boldsymbol{M})$ and the elastic stresses $\sigma_{ij} = \sigma_{ij}(\boldsymbol{M})$. Thus, σ_{ij} and ε_{ij} have a back-action on $\boldsymbol{M}$ and $\boldsymbol{M}$ should be derived by minimizing $w(\boldsymbol{M}, \varepsilon_{ij}(\boldsymbol{M}))$. In some cases, $\boldsymbol{M}$ can be approximated by $\boldsymbol{M}'$, which is obtained through minimizing $w(\boldsymbol{M}, \varepsilon_{ij} = 0)$. The difference between the approximate solution $\boldsymbol{M}'$ and rigorous solution $\boldsymbol{M}$ depends on the magnitude of the relative coefficient $\frac{K^2}{2\alpha_2(C_{11}+2C_{12})M_s^4}$ [24]. For MnSi, $\frac{K^2}{2\alpha_2(C_{11}+2C_{12})M_s^4} \approx 10^{-3}$, suggesting that the back-action of strains on the magnetization can be neglected.

As mentioned in section 3 the surface-induced stress field is just the opposite of the skyrmion-induced stress field at the surface, and it fades away as $|z|$ increases. Following the above discussion, such a localized elastic field will also have a back-action on the magnetization $\boldsymbol{M}$. Generally speaking, the z-dependent surface-induced stress field will destroy the 2D structure of the skyrmion lattice and makes it a 3D texture [30, 39]. The surface-induced stress field is maximum at the surface, whose magnitude is equivalent to the skyrmion-induced stress field. According to above analysis, the back-action on $\boldsymbol{M}$ is negligible when $\frac{K^2}{2\alpha_2(C_{11}+2C_{12})M_s^4}$ is small enough. When $\frac{K^2}{2\alpha_2(C_{11}+2C_{12})M_s^4}$ is comparable to 1 (e.g. for materials with strong magnetoelastic coupling), the back-action of the surface-induced stress field on the magnetization has to be taken into account. Instead of solving the exact 3D distribution of $\boldsymbol{M}$, we provide here an approximate method to calculate the effect of this back-action. The exact solution of magnetization $\boldsymbol{M}$ is obtained by minimizing $w(\boldsymbol{M}, \varepsilon_{ij}^{\text{skyrmion}}(\boldsymbol{M}) + \varepsilon_{ij}^{\text{surface}}(\boldsymbol{M}, z))$, where $\varepsilon_{ij}^{\text{surface}}(\boldsymbol{M}, z)$ are the surface-induce elastic strains and $\varepsilon_{ij}^{\text{skyrmion}}(\boldsymbol{M})$ are the skyrmion-induced elastic strains. Since $\varepsilon_{ij}^{\text{surface}}(\boldsymbol{M}, z)$ decrease exponentially with z, we can overestimate the effect of surface-induced elastic strains by replacing $\varepsilon_{ij}^{\text{surface}}(\boldsymbol{M}, z)$ with $\varepsilon_{ij}^{\text{surface}}(\boldsymbol{M}, 0)$. Minimization of $w(\boldsymbol{M}, \varepsilon_{ij}^{\text{skyrmion}}(\boldsymbol{M}) + \varepsilon_{ij}^{\text{surface}}(\boldsymbol{M}, 0))$ with respect to $\boldsymbol{M}$ yields a 2D magnetization distribution where the back-action of the surface-induced elastic field is considered approximately.

The discussion of the back-action on the magnetization only applies to the internal elastic field but not the external. The former one refers to the elastic field induced by $\boldsymbol{M}$ through the magnetoelastic interaction and has a back-action on $\boldsymbol{M}$. The later one is induced by external applied forces or misfit strains, and thus its influence on $\boldsymbol{M}$ is not a back-action. The magnitude of such an influence depends on the strength of the applied external field and usually cannot be ignored.

Appendix B. Two-dimensional half space elastic problem of cubic crystals

Consider a semi-infinite domain defined by $z \leqslant 0$ illustrated in figure B1, where O-xyz system is generated by rotating O-$r_1r_2r_3$ system around r_3-axis with θ; $Q(x)$ and $P(x)$ represent respectively the normal and the shear force distributions on the surface $z = 0$. For Q-induced 2D plane strain problem,we introduce the Airy stress function U so that

$$\begin{aligned}\sigma_{11} &= U_{,33}, \\ \sigma_{33} &= U_{,11}, \\ \sigma_{13} &= -U_{,13},\end{aligned} \tag{B.1}$$

where σ_{ij} are stresses and $U_{,ij} = \frac{\partial^2 U}{\partial x_i \partial x_j}$ (x_1, x_2 and x_3 represent x, y and z, respectively). The boundary condition can be then expressed as

$$(\sigma_{33})_{z=0} = (U_{,11})_{z=0} = Q(x). \tag{B.2}$$

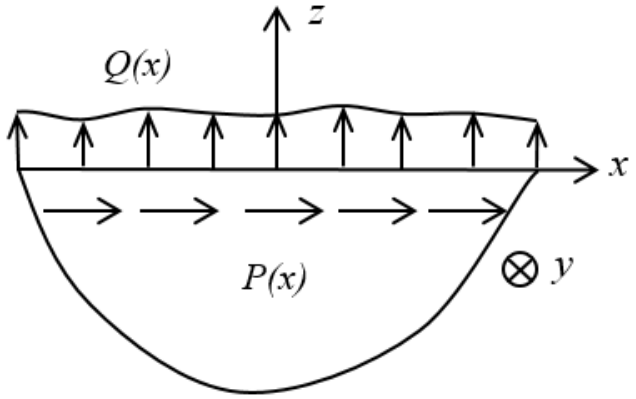

Figure B1. Semi-infinitely extended cubic crystal subjected to surface normal force $Q(x)$ and surface shear force $P(x)$.

By combining Hooke's law for cubic crystals, equation of compatibility $\varepsilon_{11,33}+\varepsilon_{33,11}=2\varepsilon_{13,13}$, and formulae (B.1), we can derive

$$\beta^4 U_{,1111}+2\mu U_{,1133}+U_{,3333}=0. \tag{B.3}$$

Here, μ and β are parameters related to the rotation angle θ and the elastic coefficients. Applying Fourier transform $\mathscr{F}$, defined as $\mathscr{X}(\lambda,z)=\mathscr{F}(X(x,z))=\frac{1}{\sqrt{2\pi}}\int_{-\infty}^{+\infty}X(x,z)e^{i\lambda x}\mathrm{d}x$, to compatibility condition (B.3) and boundary condition (B.2), we have

$$\mathscr{U}_{,3333}-2\mu'\lambda'^2\mathscr{U}_{,33}+\lambda'^4\mathscr{U}=0, \tag{B.4}$$

$$-\lambda^2(\mathscr{U})_{z=0}=\mathscr{Q}(\lambda), \tag{B.5}$$

where $\mathscr{U}$ and $\mathscr{Q}$ are the Fourier integral forms of U and Q respectively; $\mu'=\frac{\mu}{\beta^2}$ and $\lambda'=\beta\lambda$. According to the boundedness condition of $\mathscr{U}$ and the boundary condition (B.5), one arrives at

$$\mathscr{U}=\frac{\mathscr{Q}(\lambda)}{\lambda^2(t_1-t_2)}(t_2\mathrm{e}^{t_1|\lambda'|z}-t_1\mathrm{e}^{t_2|\lambda'|z}), \tag{B.6}$$

where $t_1=\sqrt{\frac{(1+\mu')}{2}}+\sqrt{\frac{(1-\mu')}{2}}\mathrm{i}$, $t_2=\sqrt{\frac{(1+\mu')}{2}}-\sqrt{\frac{(1-\mu')}{2}}\mathrm{i}$. By applying the convolution theorem to Fourier integral form of stresses, we obtain

$$\begin{aligned}
\sigma_{11}&=\frac{1}{\pi}\int_{-\infty}^{+\infty}\frac{-\beta^2\sqrt{2(1+\mu')}z'(x-\xi)^2Q(\xi)}{(x-\xi)^4+z'^4+2(x-\xi)^2z'^2\mu'}\mathrm{d}\xi,\\
\sigma_{33}&=\frac{1}{\pi}\int_{-\infty}^{+\infty}\frac{-\sqrt{2(1+\mu')}z'^3Q(\xi)}{(x-\xi)^4+z'^4+2(x-\xi)^2z'^2\mu'}\mathrm{d}\xi,\\
\sigma_{13}&=\frac{1}{\pi}\int_{-\infty}^{+\infty}\frac{-\beta\sqrt{2(1+\mu')}z'^2(x-\xi)Q(\xi)}{(x-\xi)^4+z'^4+2(x-\xi)^2z'^2\mu'}\mathrm{d}\xi,
\end{aligned} \tag{B.7}$$

where $z'=\beta z$. For isotropic materials and $\theta=0$, we have $\beta=\mu=1$, the solution for stresses (B.7) can be found in [40].

The Green's function method, which requires firstly $Q=\delta_0$ with δ the Dirac Delta function, is used to derive the solution of displacement field caused by an arbitrary $Q(x)$. The relation between displacements and stresses is obtained from Hook's law and geometric equations $\varepsilon_{ij}=\frac{u_{i,j}+u_{j,i}}{2}$,

$$\begin{aligned}
u_{1,1}&=S_{11}\sigma_{11}+S_{13}\sigma_{33},\\
u_{3,3}&=S_{31}\sigma_{33}+S_{33}\sigma_{33},
\end{aligned} \tag{B.8}$$

$$u_{1,3}+u_{3,1}=S_{44}\sigma_{13}. \tag{B.9}$$

Here, $S_{11}=\frac{C_{33}}{C_{11}C_{33}-C_{13}^2}$, $S_{13}=S_{31}=-\frac{C_{13}}{C_{11}C_{33}-C_{13}^2}$, $S_{33}=\frac{C_{11}}{C_{11}C_{33}-C_{13}^2}$ and $S_{44}=\frac{1}{C_{44}}$ with C_{ij} the elastic coefficients in O-xyz system; the stresses are obtained by applying $Q=\delta_0$ into equations (B.7). Then we derive the displacement field from equations (B.8)

$$\begin{aligned}
u_1&=S_{11}u_{11}+S_{13}u_{12}+u_{13},\\
u_3&=S_{31}u_{31}+S_{33}u_{32}+u_{33}.
\end{aligned} \tag{B.10}$$

u_{13} is a function of z, u_{33} is a function of x and

$$\begin{aligned}
u_{11}&=\frac{\beta^2}{4\pi}\sqrt{\frac{1+\mu'}{1-\mu'}}\ln\left(\frac{z'^2+x^2+xz'\sqrt{2(1-\mu')}}{z'^2+x^2-xz'\sqrt{2(1-\mu')}}\right)-\frac{\beta^2}{2\pi}\arctan\left(\frac{xz'\sqrt{2(1+\mu')}}{z'^2-x^2}\right)+\frac{\beta^2}{2}\left(\mathrm{H}_{z'}(2z'-x)-\mathrm{H}_{-z'}(x)\right),\\
u_{12}&=-\frac{1}{2\pi}\arctan\left(\frac{xz'\sqrt{2(1+\mu')}}{z'^2-x^2}\right)-\frac{1}{4\pi}\sqrt{\frac{1+\mu'}{1-\mu'}}\ln\left(\frac{z'^2+x^2+x'z\sqrt{2(1-\mu')}}{z'^2+x^2-xz'\sqrt{2(1-\mu')}}\right)+\frac{1}{2}(\mathrm{H}_{z'}(2z'-x)-\mathrm{H}_{-z'}(x)),\\
u_{31}&=-\frac{\beta}{\pi}\sqrt{\frac{1}{2(1-\mu')}}\arctan\left(\frac{\sqrt{1-\mu'^2}z'^2}{x^2+\mu'z'^2}\right),\\
u_{32}&=-\frac{\sqrt{2(1+\mu')}}{4\pi\beta}\ln(z'^4+x^4+2z'^2x^2\mu)-\frac{\mu'}{\pi\beta\sqrt{2(1-\mu')}}\arctan\left(\frac{\sqrt{1-\mu'^2}x^2}{z'^2+\mu'x^2}\right),
\end{aligned} \tag{B.11}$$

where $\mathrm{H}_{z'}(x)$ is defined as $\mathrm{H}_{z'}(x)=\mathrm{H}(x-z')$,with $\mathrm{H}(x)=\frac{1+\mathrm{sgn}(x)}{2}$ the Heaviside step function. The Heaviside

step functions are added in formulae (B.11) to ensure the continuity of displacement field on points $x = z'$ and $x = -z'$.

By substituting equations (B.10) and (B.11) into equation (B.9), we get the following differential equation with a very simple form

$$\frac{\mathrm{d}u_{13}(z)}{\mathrm{d}z} + \frac{\mathrm{d}u_{33}(x)}{\mathrm{d}x} = 0, \tag{B.12}$$

which has the solution $u_{13} = kz + m, u_{33} = -kx + n$, with k, m and n constants. The meaning of k is that the material rotates around y-axis with an angle $-\arctan(k)$, and then enlarges it's volume $(1 + k^2)^{\frac{3}{2}}$ times. m and n represent the rigid body movement. Set $k = m = n = 0$, we have

$$\begin{aligned} u_1 &= S_{11}u_{11} + S_{13}u_{12}, \\ u_3 &= S_{31}u_{31} + S_{33}u_{32}. \end{aligned} \tag{B.13}$$

Consequently, the displacement field for arbitrary surface force distribution $Q(x)$ can be easily obtained, from eqs. (B.13)

$$\begin{aligned} u_1 &= \int_{-\infty}^{+\infty} (S_{11}u_{11}(\xi, z) + S_{13}u_{12}(\xi, z))Q(x - \xi)\mathrm{d}\xi, \\ u_3 &= \int_{-\infty}^{+\infty} (S_{31}u_{31}(\xi, z) + S_{33}u_{32}(\xi, z))Q(x - \xi)\mathrm{d}\xi. \end{aligned} \tag{B.14}$$

By using the same method, we can derive the displacement field induced by the shear force distribution $P(x)$ as:

$$\begin{aligned} u_1 &= \int_{-\infty}^{+\infty} (S_{11}u'_{11}(\xi, z) + S_{13}u'_{12}(\xi, z))Q(x - \xi)\mathrm{d}\xi, \\ u_3 &= \int_{-\infty}^{+\infty} (S_{31}u'_{31}(\xi, z) + S_{33}u'_{32}(\xi, z))Q(x - \xi)\mathrm{d}\xi \end{aligned} \tag{B.15}$$

where

$$\begin{aligned} u'_{11} = &-\frac{\beta^2\mu'}{\pi\sqrt{2(1-\mu')}}\arctan\left(\frac{\sqrt{1-\mu'^2}z'^2}{x^2+\mu'z'^2}\right) - \frac{\beta^2\sqrt{2(1+\mu')}}{4\pi} \\ &\ln(z'^4 + x^4 + 2z'^2x^2\mu'), u'_{12} = -\frac{u_{31}}{\beta}, \ u'_{31} = -\frac{u_{11}}{\beta}, \ u'_{32} = -\frac{u_{12}}{\beta}. \end{aligned} \tag{B.16}$$

We now consider a simple case when $\theta = 0$ and the semi-infinite cubic crystal is subjected to an evenly distributed normal force on the surface, $Q = 1$. Obviously, the displacement field along z-axis is linear with z: $u_3(x, z) = kz$ (solution 1), where k is a constant merely related to elastic moduli. But on the other hand, via the formulae (B.14), one arrives at

$$u_3(x, z) = \int_{-\infty}^{+\infty} (S_{31}u_{31}(\xi, z) + S_{33}u_{32}(\xi, z))\mathrm{d}\xi, \tag{B.17}$$

(solution 2). We find that solution 1 and solution 2 are not the same; moreover, the integral form of solution 2 is divergent. In fact, the difference between those two solutions originates from the choice of the fixed plane: solution 1 is obtained under the assumption that the plane $z = 0$ is fixed, while solution 2 is gotten with the plane $z = +\infty$ fixed. According to the theory of elasticity, such difference (even though infinite) can be seen as a constant. To eliminate this special constant, we calculate the finite part of the divergent integral (B.17) by using the method of functional regularization of general function which regards the order of differential and integral as exchangeable [41]. We first calculate the partial derivative of solution 2 with respect to z, and then, integrate the obtained partial derivative with respect to z. The result, $u_3(x, z) = -\frac{z}{C_{11}-C_{12}}$, has the same form as solution 1. Thus, from a physics point of view, the mathematical difficulty is just due to the choice of reference system, and it can be solved by translating the reference system along z-axis with an infinite distance. Mathematically, the method is related to the calculation of the finite part of the divergent integral.

ORCID iDs

Yangfan Hu https://orcid.org/0000-0001-8954-4028

References

[1] Múhlbauer S, Binz B, Jonietz F, Pfleiderer C, Rosch A, Neubauer A, Georgii R and Bóni P 2009 Skyrmion lattice in a chiral magnet *Science* **323** 915–9

[2] Petrova O and Tchernyshyov O 2011 Spin waves in a skyrmion crystal *Phys. Rev.* B **84** 214433

[3] Hu Y 2017 Wave-nature and intrinsic stability of emergent crystals in chiral magnets (arXiv:1702.01059)

[4] Bogdanov A N and Yablonskii D A 1989 Thermodynamically stable 'vortices' in magnetically ordered crystals. The mixed state of magnets *Sov. Phys. JETP* **68** 101–3

[5] Bogdanov A and Hubert A 1994 Thermodynamically stable magnetic vortex states in magnetic crystals *J. Magn. Magn. Mater.* **138** 255–69

[6] Moskvin E, Grigoriev S, Dyadkin V, Eckerlebe H, Baenitz M, Schmidt M and Wilhelm H 2013 Complex chiral modulations in fege close to magnetic ordering *Phys. Rev. Lett.* **110** 077207

[7] Münzer W *et al* 2010 Skyrmion lattice in the doped semiconductor $Fe_{1-x}Co_xSi$ *Phys. Rev.* B **81** 041203

[8] Shibata K, Yu X Z, Hara T, Morikawa D, Kanazawa N, Kimoto K, Ishiwata S, Matsui Y and Tokura Y 2013 Towards control of the size and helicity of skyrmions in helimagnetic alloys by spin–orbit coupling *Nat. Nanotechnol.* **8** 723–8

[9] Tokunaga Y, Yu X Z, White J S, Rønnow H M, Morikawa D, Taguchi Y and Tokura Y 2015 A new class of chiral materials hosting magnetic skyrmions beyond room temperature *Nat. Commun.* **6** 7638

[10] Rößler U K, Bogdanov A N and Pfleiderer C 2006 Spontaneous skyrmion ground states in magnetic metals *Nature* **442** 797–801

[11] Jonietz F *et al* 2010 Spin transfer torques in mnsi at ultralow current densities *Science* **330** 1648–51

[12] Seki S, Ishiwata S and Tokura Y 2012 Magnetoelectric nature of skyrmions in a chiral magnetic insulator Cu_2OSeO_3 *Phys. Rev.* B **86** 060403

[13] Kiselev N S, Bogdanov A N, Schäfer R and Rößler U K 2011 Chiral skyrmions in thin magnetic films: new objects for magnetic storage technologies? *J. Phys. D: Appl. Phys.* **44** 392001

[14] Kosevich A M, Ivanov B A and Kovalev A S 1981 Dynamical and topological solitons in a ferromagnet *Physica* D **3** 363–73

[15] Kosevich A M, Ivanov B A and Kovalev A S 1990 Magnetic solitons *Phys. Rep.* **194** 117–238

[16] Onose Y, Okamura Y, Seki S, Ishiwata S and Tokura Y 2012 Observation of magnetic excitations of skyrmion crystal in a helimagnetic insulator Cu_2OSeO_3 *Phys. Rev. Lett.* **109** 037603
[17] Yu X, Kikkawa A, Morikawa D, Shibata K, Tokunaga Y, Taguchi Y and Tokura Y 2015 Variation of skyrmion forms and their stability in mnsi thin plates *Phys. Rev.* B **91** 054411
[18] Nii Y, Nakajima T, Kikkawa A, Yamasaki Y, Ohishi K, Suzuki J, Taguchi Y, Arima T, Tokura Y and Iwasa Y 2015 Uniaxial stress control of skyrmion phase *Nat. Commun.* **6** 8539
[19] Chacon A, Bauer A, Adams T, Rucker F, Brandl G, Georgii R, Garst M and Pfleiderer C 2015 Uniaxial pressure dependence of magnetic order in mnsi *Phys. Rev. Lett.* **115** 267202
[20] Nii Y, Kikkawa A, Taguchi Y, Tokura Y and Iwasa Y 2014 Elastic stiffness of a skyrmion crystal *Phys. Rev. Lett.* **113** 267203
[21] Shibata K *et al* 2015 Large anisotropic deformation of skyrmions in strained crystal *Nat. Nanotechnol.* **10** 589–92
[22] Hu Y and Wang B 2016 Reversible triple elastic field structures in a chiral magnet *Sci. Rep.* **6** 30200
[23] Stishov S M, Petrova A E, Khasanov S, Panova G K, Shikov A A, Lashley J C, Wu D and Lograsso T A 2008 Experimental study of the magnetic phase transition in the mnsi itinerant helimagnet *J. Exp. Theor. Phys.* **106** 888–96
[24] Hu Y and Wang B 2017 Unified theory of magnetoelastic effects in b20 chiral magnets *New J. Phys.* **19** 123002
[25] Karhu E A, Rößler U K, Bogdanov A N, Kahwaji S, Kirby B J, Fritzsche H, Robertson M D, Majkrzak C F and Monchesky T L 2012 Chiral modulations and reorientation effects in mnsi thin films *Phys. Rev.* B **85** 094429
[26] Schulz T, Ritz R, Bauer A, Halder M, Wagner M, Franz C, Pfleiderer C, Everschor K, Garst M and Rosch A 2012 Emergent electrodynamics of skyrmions in a chiral magnet *Nat. Phys.* **8** 301–4
[27] Kong L and Zang J 2013 Dynamics of an insulating skyrmion under a temperature gradient *Phys. Rev. Lett.* **111** 067203
[28] Hu Y and Wang B 2016 Emergent elasticity of skyrmion lattice in chiral magnets (arXiv:1608.04840)
[29] Bogdanov A N and Rößler U K 2001 Chiral symmetry breaking in magnetic thin films and multilayers *Phys. Rev. Lett.* **87** 037203
[30] Rybakov F N, Borisov A B, Blúgel S and Kiselev N S 2015 New type of stable particlelike states in chiral magnets *Phys. Rev. Lett.* **115** 117201
[31] Heinze S, Von Bergmann K, Menzel M, Brede J, Kubetzka A, Wiesendanger R, Bihlmayer G and Blúgel S 2011 Spontaneous atomic-scale magnetic skyrmion lattice in two dimensions *Nat. Phys.* **7** 713–8
[32] Ezawa M 2010 Giant skyrmions stabilized by spin–orbit interactions in thin ferromagnetic films *Phys. Rev. Lett.* **105** 197202
[33] Kirakosyan A S and Pokrovsky V L 2006 From bubble to skyrmion: dynamic transformation mediated by a strong magnetic tip *J. Magn. Magn. Mater.* **305** 413–22
[34] Abanov A and Pokrovsky V L 1998 Skyrmion in a real magnetic film *Phys. Rev.* B **58** R8889
[35] Ivanov B A and Stephanovich V A 1989 Two-dimensional soliton dynamics in ferromagnets *Phys. Lett.* A **141** 89–94
[36] Kézsmárki I *et al* 2015 Néel-type skyrmion lattice with confined orientation in the polar magnetic semiconductor GaV_4S_8 *Nat. Mater.* **14** 1116–22
[37] Huang S X and Chien C L 2012 Extended skyrmion phase in epitaxial FeGe (1 1 1) thin films *Phys. Rev. Lett.* **108** 267201
[38] Yu X Z, Kanazawa N, Onose Y, Kimoto K, Zhang W Z, Ishiwata S, Matsui Y and Tokura Y 2011 Near room-temperature formation of a skyrmion crystal in thin-films of the helimagnet fege *Nat. Mater.* **10** 106–9
[39] Rybakov F N, Borisov A B, Blúgel S and Kiselev N S 2016 New spiral state and skyrmion lattice in 3D model of chiral magnets *New J. Phys.* **18** 045002
[40] Timoshenko S P and Goodier J N 1970 *Theory of Elasticity* (New York: McGraw-Hill)
[41] Wang M Z 1985 Application of the finite part of a divergent integral in the theory of elasticity *Appl. Math. Mech.* **6** 1071–8